CONF-9

January 1993

BNL--47691

DE93 009343

POTENTIAL APPLICATIONS OF SYNCHROTRON COMPUTED MICROTOMOGRAPHY TO SOIL SCIENCE

P. Spanne, K. W. Jones

Brookhaven National Laboratory, Upton, New York 11973

L. D. Prunty

North Dakota State University, Fargo, North Dakota 58105

S. H. Anderson

University of Missouri-Columbia, Columbia, MO 65211

Presented at

1992 Annual Meetings of the

American Society of Agronomy, Crop Science Society of America, and

Soil Science Society of America

Minneapolis, Minnesota

November 1-6, 1992

Potential Applications of Synchrotron Computed Microtomography to Soil Science

P. Spanne*, K.W. Jones, L. D. Prunty, and S. H. Anderson

P. Spanne and K. W. Jones, Department of Applied Science, Building 815, Brookhaven National Laboratory, Upton, NY 11973; L. D. Prunty, 147 Walster Hall, Department of Soil Science, North Dakota State University, Fargo, ND 58105; and S. H. Anderson, 144 Mumford Hall, The School of Natural Resources, Soil Science, University of Missouri-Columbia, Columbia, MO 65211. Work supported in part by the US DOE under Contract No. DE-AC02-76CH00016. *Corresponding author.

ABSTRACT

Synchrotron x-ray computed microtomography (CMT) can be used to make non-destructive tomographic sections with spatial resolutions of a few μm. This resolution presents possibilities for study of soil-fluid interactions on a spatial scale hitherto unreachable. Details of a CMT apparatus in operation at the Brookhaven National Synchrotron Light Source X26 beam line are presented and prospects for future development at new synchrotron facilities are considered. Several investigations of test systems have been made and results for wet and dry samples of glass beads and sand samples are given to show the power of the system.

Additional Index Words: computed microtomography, synchrotron radiation

INTRODUCTION

There is great interest in measurement of bulk density and water content of soils on length scales from the microscopic (micrometers) to the macroscopic (centimeters). The information derived from these measurements is essential for understanding fluid flow, transport of toxic materials, and soil-root water transport. The means for making such determinations have been non-existent in the past.

Recently, however, computed tomography has been applied to the nondestructive evaluation of soil-water samples (Crestana et al., 1985; Hainsworth and Aylmore, 1986; Anderson et al., 1988). These and other studies demonstrated that bulk densities can be measured and that kinetic studies can be made on movement of water in soils.

Tomographic imaging with spatial resolutions on the micrometer scale in a reasonable length of time has only become possible with the construction of synchrotron radiation x-ray sources. The development of micrometer resolution computed microtomography (CMT) apparatus has taken place during the past 5-10 years (e. g. Flannery, et al., 1987; Spanne and Rivers, 1987; Kinney, et al., 1990; Jones, et al., 1992). Resolutions close to 1 μm have been achieved which can be exploited for soil physics experiments.

The present paper describes the parameters of the synchrotron x-ray source, discusses possible applications in soil physics studies, and presents tomograms of several specimens, both dry and wet.

APPLICATIONS OF CMT TO SOIL SCIENCE

Fundamental understanding of transport processes in soil is essential if progress is to be made toward solution of important environmental problems. The geometry of liquid films in soil pores a few μm in diameter influences numerous important processes, e.g., transport of water and nutrients to plant roots and migration of toxic and hazardous substances in soil. Another example where liquid film geometry influences an important process in soil is in diffusion of oxygen to microbes that can break down soil contaminants.

Contaminants of concern in soil include pesticides, volatile organic compounds (VOCs), nonaqueous phase liquids (NAPL), and salts. These materials may be present in soil either through accidental spillage, intentional application, or disposal activities. The location of liquid phases of water and contaminants that are immiscible in water influence degradation mechanisms, pathways, and flow rates.

The spatial arrangement of liquids at the pore scale in unsaturated soil is essentially unknown. The relative locations of water and NAPL have been studied to a limited extent in relation to extraction of oil from geologic formations. However, these are generally saturated systems and do not relate to unsaturated situations that are typical of pesticide, VOC, or NAPL contamination. Examples of specific observations that will provide important information if made at the pore scale are: contact angles of the liquids and contact angle variation on different soil particles; curvature of liquid-liquid and liquid-air interfaces as compared to theory; regions of non-wetting; and evidence of hysteretic effects.

The redistribution of water and octane in soil in the presence of a thermal gradient was recently investigated (Prunty, 1992) with resolution on the cm scale. Observations from similar experiments on the sub-mm scale in real time could lead to much-improved understanding of and ability to computer model such systems. Recent work (Wilson et al., 1989) to observe multiphase displacement processes in saturated pore networks used two-dimensional etched-glass micromodels with typical pore dimensions of about 500 μm. However, pore sizes of interest for unsaturated flow in many real soils are smaller than this by factors of 10 or more.

Presently, there is an absence of direct observation of liquid films that surround soil particles. Meniscus effects caused by surface tension and similar to those observable directly at larger scales, in glass tubes for instance, have been presumed to also act at the scale of soil pores. CMT offers the possibility of direct observation of the liquid films in soil pores with sizes corresponding to the lower range of silt particle diameters. An important need for observations at this scale can therefore be filled by CMT.

THEORETICAL BACKGROUND

The incentive for making the CMT investigation is the opportunity to test the theoretical concepts believed to govern the behavior of water in small soil pores. Theoretically, it is thought that water is distributed over solid particles in unsaturated solid soil in a manner according to a surface tension model (at least in the region where capillary tension is less than about 100 kPa). However, the curvature of water films in these systems has never been observed directly. Direct observation is necessary to test the adequacy of this assumption.

Further, the relationship for capillary pressure, p, is $p = 2\ s/r$ where s is surface tension and r is radius of curvature of the water film. The quantity 2/r is known as the total curvature and is the sum of the inverse of radii of plane curves created by the intersection of the surface in question and two perpendicular planes (Kirkham and Powers, 1972). If soil water is in equilibrium throughout a volume of soil then the capillary pressure should be the same everywhere and, hence, the curvature of water film surfaces should also be the same everywhere. Calculations based on the equation show that at $r = -20\ \mu m$ the capillary pressure p will be about -7 kPa. Similarly, at $r = -1\ \mu m$, $p = -150$ kPa. This range of pressure (matric potential) is within the primary region of interest for plant growth and the corresponding radii should be readily observable in CMT sections taken with pixel sizes of a few μm and less.

THE SYNCHROTRON X-RAY SOURCE

The properties of the synchrotron x-ray source are the key to successful CMT. The present work was carried out at the X26 beam lime of the National Synchrotron Light Source (NSLS) x-ray ring. This source operates at an energy of 2.5 GeV with stored electron currents ranging from about 250 mA at injection to about 110 mA at the end of a fill. The key parameter is the brightness of the source often specified as the number of photons emitted from the x-ray source into infinitesimal vertical and horizontal angles for a 1 eV x-ray energy bandwidth and 1 mA stored electron current in the ring. A high brightness ensures that it will be possible to produce a beam with high photon fluence rate at a sample some meters from the ring. It is important to stress that the brightness of the NSLS synchrotron x-ray source is 3-4 orders of magnitude higher than the brightness of conventional x-ray tubes. This makes possible the implementation of CMT with resolutions superior to those produced by systems based on conventional x-ray tubes. Furthermore, the next generation of synchrotron sources will see another increment of 3-4 orders of magnitude produced by undulator insertion devices. Examples of third-generation sources are the Advanced Photon Source (APS) now being constructed at Argonne National Laboratory and the European Synchrotron Radiation Facility (ESRF) in Grenoble, France. In addition, synchrotron sources produce x-rays which (1) are highly polarized; (2) are emitted with low angular divergence that results in nearly parallel beams; and (3) have a continuous energy spectrum with useable fluence rates up to an energy that depends on the storage ring, but can exceed 100 keV.

The brightness for several types of synchrotron sources is shown in Fig. 1. In the CMT work done at BNL we have often employed a filtered x-ray beam. A metal filter made of a material with the K photoelectric absorption edge close to the optimum x-ray energy for CMT (Spanne, 1989) of the sample was then used to shape the energy spectrum appropriately with regard to sample size and composition. Such a filter results in a roughly triangular x-ray spectrum with a relatively large full-width-at-half maximum of about 10%.

The broad energy distribution makes it difficult to obtain accurate linear attenuation coefficients but has the advantage of giving a very high photon fluence rate. At the X26 beam line, the photon fluence rate per 100 mA ring current through a pinhole located 10 m from the x-ray source is about 10^8 photons/($\mu m^2 \cdot s \cdot 100$). This is sufficient to make measurements on the micrometer scale.

EXPERIMENTAL PROCEDURES

NSLS X26 CMT Apparatus

The CMT apparatus was used in a first generation configuration. This approach is advantageous for reducing artifacts caused by scattered radiation reaching the x-ray detector and also makes it feasible to make tomographic sections based on the detection of characteristic x-rays, so-called emission CMT. Thus, the distribution of particular trace elements on different types of soil particles could be mapped. The drawback of the first generation configuration is the length of time (about 60 minutes for a 500 × 500 picture elements image with a voxel size of 8 μm^3) needed to accumulate data for a complete image. Use of detector arrays where all rays are measured at the same time for a given angle of view gives greatly reduced imaging times, typically less than one minute for a complete tomographic section.

We used a collimator constructed from Ta flats to produce pencil beams with areas down to a few micrometers. An assembly of computer-controlled stepper motor driven translators and rotators was used to align the collimator opening with the x-ray beam. The primary x-ray beam emerging through the exit window of the beam line pipe was filtered by 100 μm Mo before the specimen. The x-ray beam transmitted by the sample was detected with a CaF_2 scintillator viewed by a photomultiplier tube operated in current mode. The detector signal was digitized and used to calculate estimates of the line integrals of the linear attenuation coefficients for the ray paths through the specimen. The line integrals, determined as a function of the position of the pencil beam on the specimen and the angular

position of the specimen with respect to the beam, were used for the tomographic image reconstruction, which was a filtered back-projection algorithm (Herman, 1980).

Preparation of Samples

The soil sample containers consisted of 1000 μl pipette tips melted shut at the small end and sealed by molten wax after filling with sample material. Image slices were taken near the end of the tapered tip where the diameter was about 2.5 mm. For some samples heat shrink plastic tubing was used since it was readily available in different diameters. Glass beads were used as test objects. Several types were measured with diameters ranging from about 37 μm to 600 μm. Sand samples with diameters from 250 μm to 500 μm were also measured. Both dry and wet samples were imaged using pure water and water plus 1% iodine by weight to enhance the contrast between the solid and liquid phases.

RESULTS AND DISCUSSION

The resolution of the CMT system is demonstrated by the tomographic sections shown in Figs. 2a and 2b. The section on the left is through grains of SiO_2. A crack can be seen in a grain to the upper right of this section. An enlarged view of that grain is shown in Fig. 2b. The width of the crack is about 6 μm. The voxel size for this image was 2 μm x 2 μm x 2 μm.

A tomographic section obtained for a sample of 100 μm glass beads (Structure Probe, Inc.) is shown in Fig. 3. The voxel size for this image was 5 μm x 5 μm x 5 μm.

An image of glass beads with diameters ranging from 425-600 μm was obtained with the beads in a 1 weight per cent solution of iodine in water. The tomogram is shown in Fig. 4, where the full contrast range from air and up is shown, and in Fig. 5 where a smaller range of pixel values are displayed to emphasize the portion of the image occupied by the fluid. Figure 5 shows that the fluid distribution was non-uniform in this portion of the specimen. The frequency of occurrence of the reconstructed linear attenuation coefficients for the tomographic section shown in Fig. 4 is plotted as a function of the reconstructed

linear attenuation coefficient in Fig. 6. Only the region occupied by the beads was used in constructing this plot. The two peaks at 200 m^{-1} and 700 m^{-1} correspond to fluid and glass regions, respectively. The voxel size was 10 μm × 10 μm × 2 μm for both figures.

A tomographic section obtained for a sand sample is shown in Fig. 7. The full contrast range was used in this image so that evidence for fluids is not visible. There is a marked non-uniformity in composition in the grains shown in these sections. It should be noted that since a pencil beam with a ~ 2 × 2 μm^2 cross sectional area was used, but the pixel site was 5 × 5 μm^2, the noise in the images is therefore characteristic for 2 μm rather than 5 μm resolution CMT.

Examination of both the tomographic sections and histograms giving the frequency distribution of the linear attenuation coefficients in the reconstructed images showed the existence of experimental artifacts that were attributed to shifting of bead positions during the tomographic measurement. This problem can be eliminated by reducting the acceleration of the sample during the rotations and translations that take place during data collection. Tapping the specimen container to ensure that the beads were in a stable configuration before starting the imaging was also beneficial.

CONCLUSIONS

The experimental results presented here show that it is feasible to obtain high quality tomograms that can be used to study interactions between soils and liquids. Future applications of computed microtomography to soil science will range from basic measurements involving fluid flow, porosity and permeability, behavior of the fluid at the solid-liquid interface to specific applied site-related problems involving different types of contaminant fluids. Further, the high spatial resolution will permit studies of the uptake of water by plant root systems under controlled conditions. Clearly, one of the first priorities would be to examine soils contaminated with several of the specific substances that cause the greatest environmental concern. For instance CCl_4 is a major concern at the USDOE

Hanford Site and leakage of gasoline from underground storage tanks has occurred at hundreds of locations in the United States. Experimental investigation of such soil samples using CMT would be of great interest for confirmation of liquid-soil interaction models.

REFERENCES

Anderson, S. H., C. J. Gantzer, J. M. Boone, and R. J. Tully. 1988. Rapid nondestructive bulk density and soil-water content determination by computed tomography. Soil Sci. Soc. Am. J. 52:35-40.

Crestana, S., S. S. Mascarenhas, and R. S. Pozzi-Mucelli. 1985. Static and dynamic three-dimensional studies of water in soil using computed tomographic scanning. Soil Sci. 140:326-332.

Flannery, B. P., H. Deckman, W. Roberge, K. D'Amico. 1987. Three dimensional x-ray microtomography. Science 237:1439-1444.

Hainsworth, J. M. and L. A. G. Aylmore. 1986. Water extraction by single plant roots. Soil Sci. Soc. Am. J. 50:841-848.

Herman, G. T. 1980. Image reconstruction from projections. The fundamentals of computerized tomography. Academic Press, New York.

Jones, K. W., Spanne, P., Lindquist, W. B., Conner, W. C., and Ferrero, M. 1992. Determination of polymerization particle morphology using synchrotron computed microtomography. Nucl. Instrum. Methods Phys. Res. B68:105-110.

Kinney, J. H., S. R. Stock, M. C. Nichols, U. Bonse, T. M. Breunig, R. A. Saroyan, R. Nusshardt, Q. C. Johnson, F. Busch, S. D. Antolovich. 1990. Nondestructive investigation of damage in composites using x-ray tomographic microscopy (XTM). J. Mater. Res. 5:1123-1129.

Kirkham, Don, and W. L. Powers. 1972. Advanced soil physics. Wiley-Interscience, New York.

Prunty, Lyle. 1992. Thermally driven water and octane redistribution in unsaturated, closed soil cells. Soil Sci. Soc. Am. J. In press.

Spanne, P. and M. L. Rivers. 1987. Computerized microtomography using synchrotron radiation from the NSLS. Nucl. Instr. Methods Phys. Res. B24/25:1063-1067.

Spanne, P. X-ray energy optimisation in computed microtomography. 1989. Phys. Med. Biol. 34:679-690.

Structure Probe, Inc., West Chester, PA 19381. Part No. 02720-AB.

Wilson, J. L., S. H. Conrad, W. R. Mason, W. Peplinski, and E. Hagan. 1989. Laboratory investigation of residual liquid organics from spills, leaks, and the disposal of hazardous wastes in groundwater. USEPA Rep. EPA/600/6-90/004 reproduced by NTIS (PB90-235797).

FIGURE CAPTIONS

Fig. 1. Energy distribution of x rays produced at the NSLS and APS storage rings. The enhancement of brightness obtained by using the undulator A at the APS is evident in the figure.

Fig. 2. Tomograms showing a) the internal structure of grains of SiO_2 and b) magnified view of a crack in a single grain (from Jones, et al., 1992). The pixel size is $2 \times 2\ \mu m^2$ and the beam height 2 μm, corresponding to a 2-μm slice thickness. The image matrix is 493 × 493 elements.

Fig. 3. Tomogram of cylindrical sample of spherical 100-μm diameter glass beads in a container made of heat shrink tubing. Low attenuation is displayed black, high attenuation white. Pixel size $5 \times 5\ \mu m^2$, slice thickness 5 μm. 601 × 601 element image matrix.

Fig. 4. Tomographic section of 425-600 μm diameter glass beads in a 1% by weight solution of iodine in water. The full contrast range is shown. Pixel size $10 \times 10\ \mu m^2$. Slice thickness 2 μm. 401 × 401 element image matrix.

Fig. 5. Same as Fig. 4, but display window has been restricted to emphasize the liquid.

Fig. 6. Histogram showing frequency of occurrence of the reconstructed linear attenuation coefficients for the tomographic section displayed in Fig. 4. Only the region occupied by the beads was considered.

Fig. 7. Tomogram through grains of sand. Pixel size $10 \times 10\ \mu m^2$, slice thickness 2 μm, 407 × 407 element image matrix.

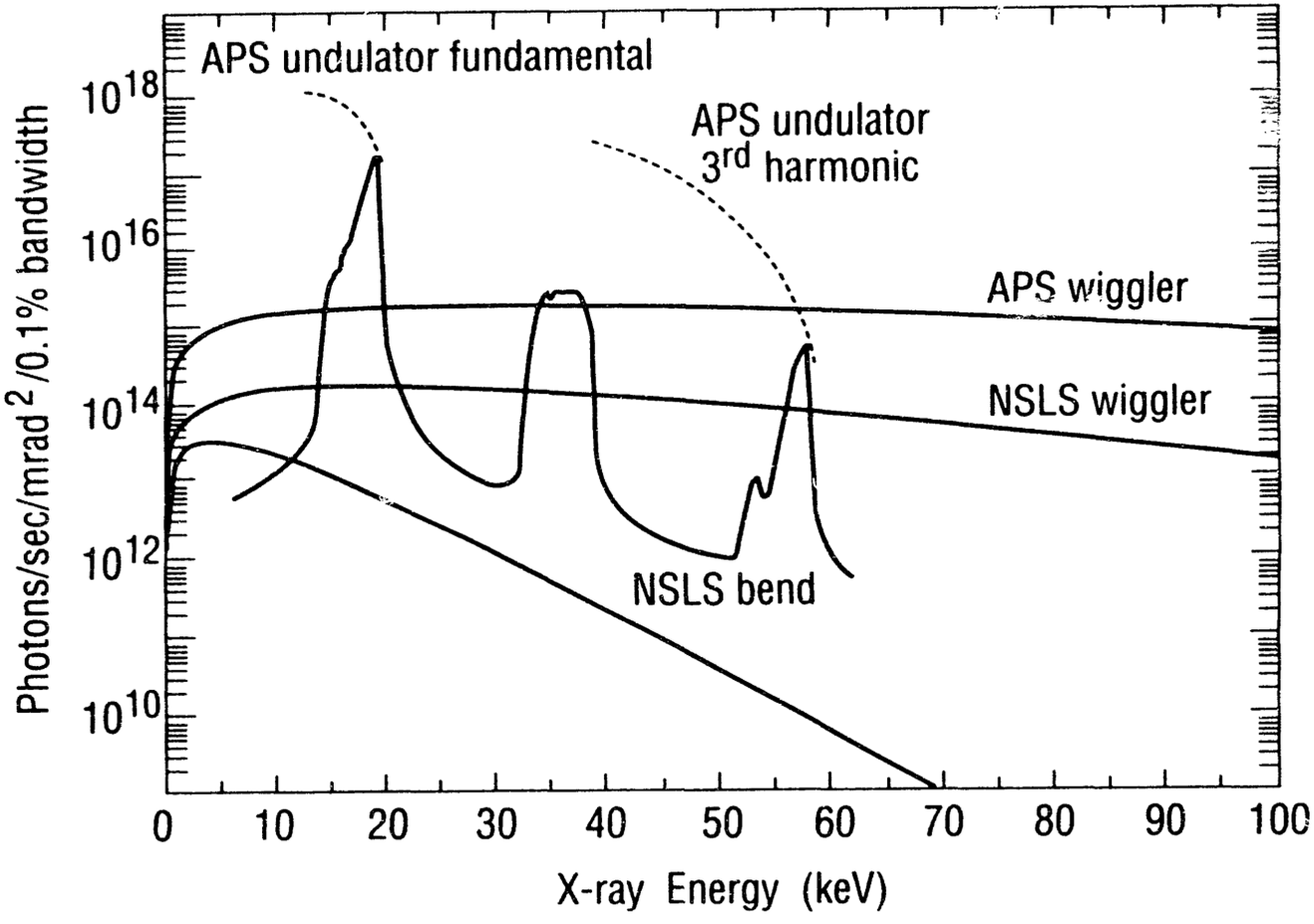

Figure 1

Jones 2 12/92 IR

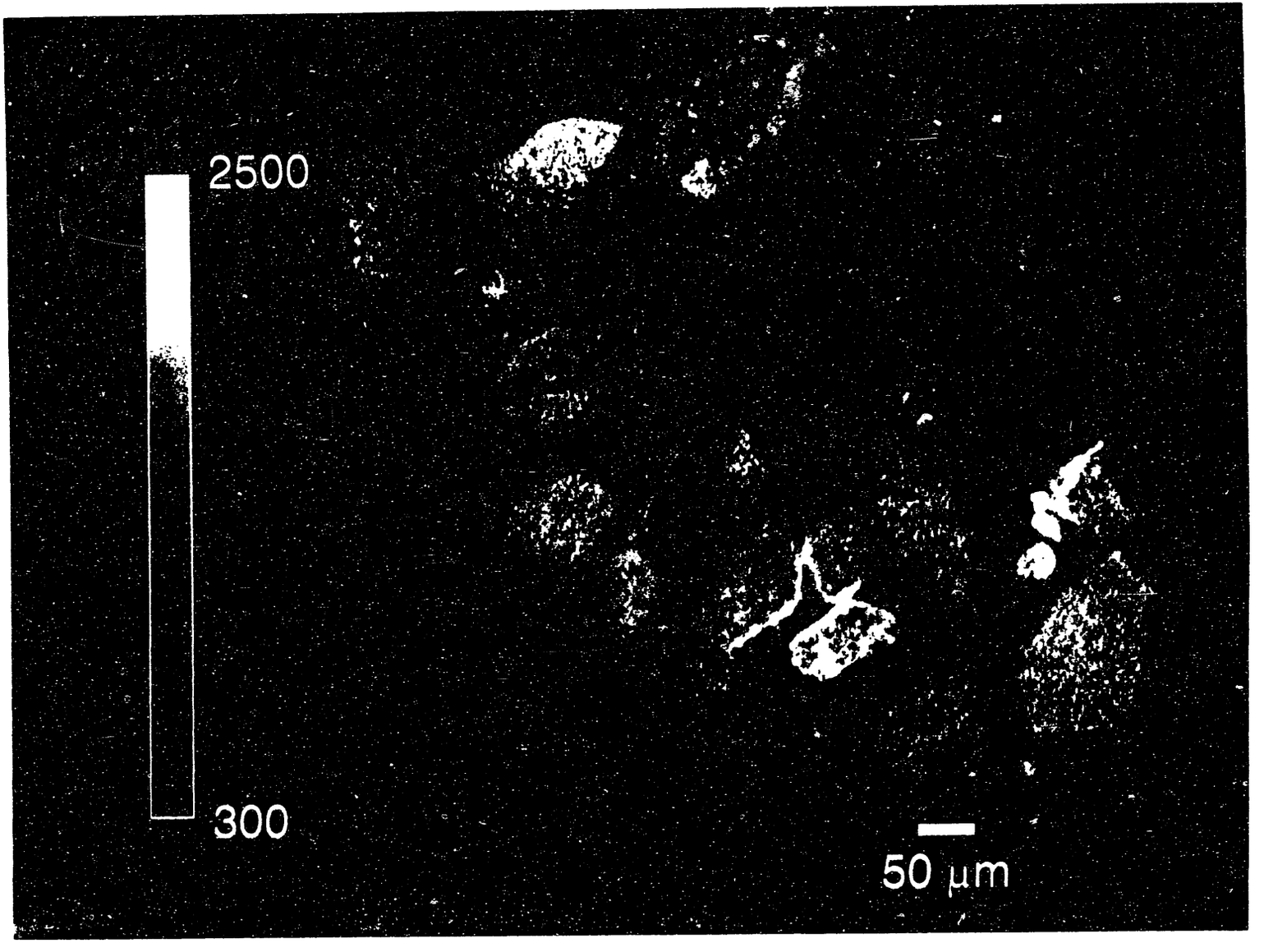

Figure 2a

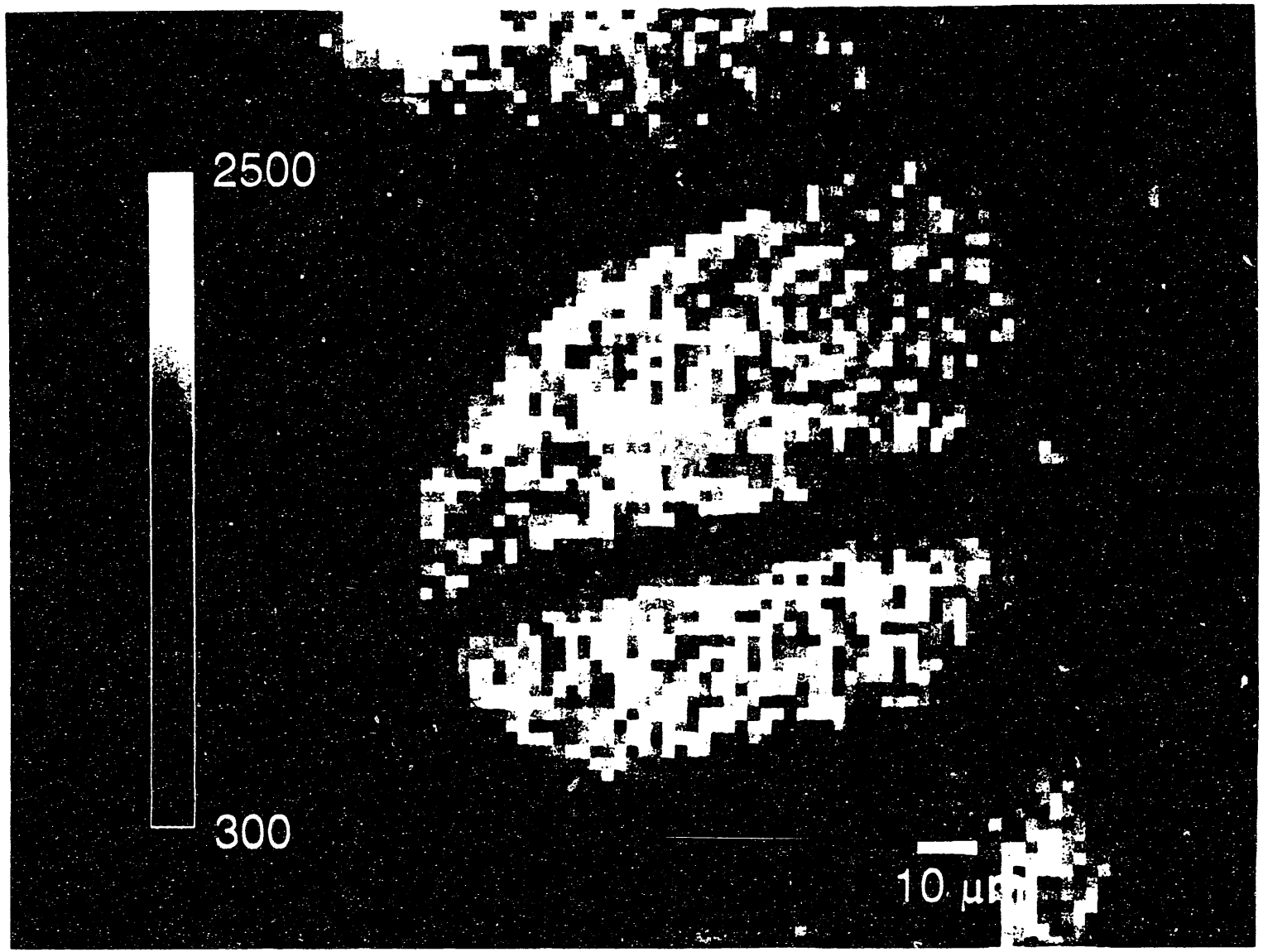

Figure 2b

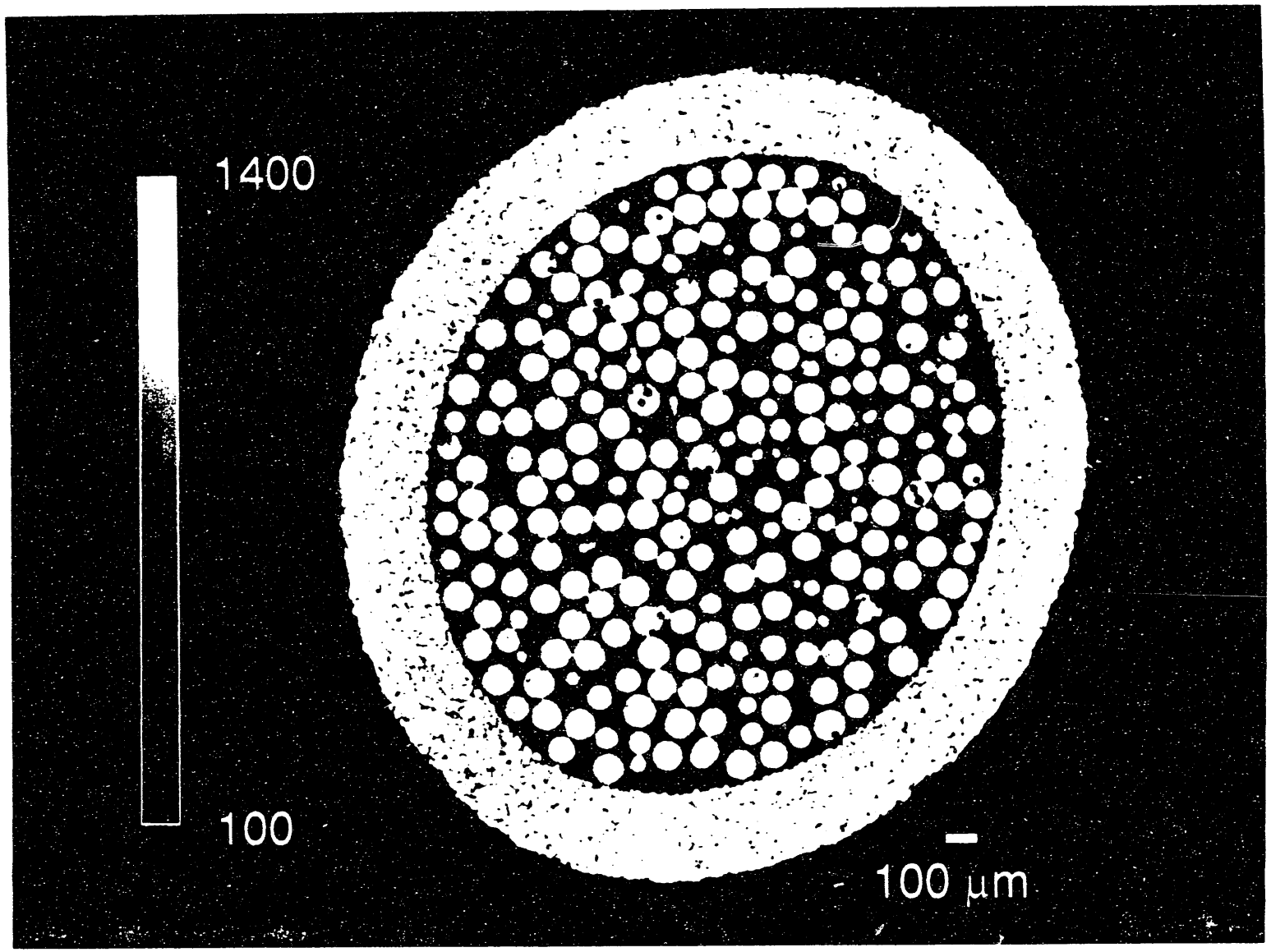

Figure 3

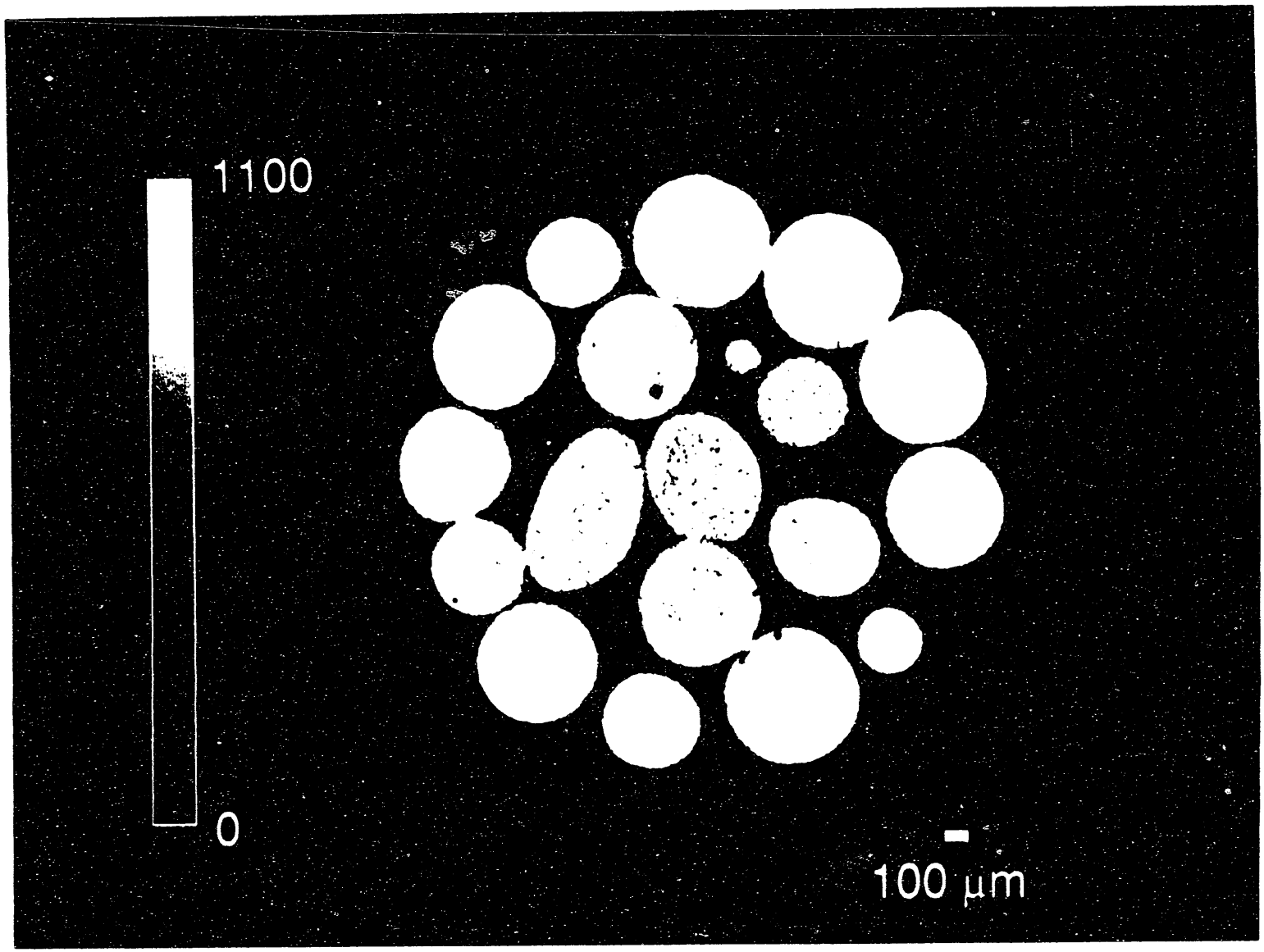

Figure 4

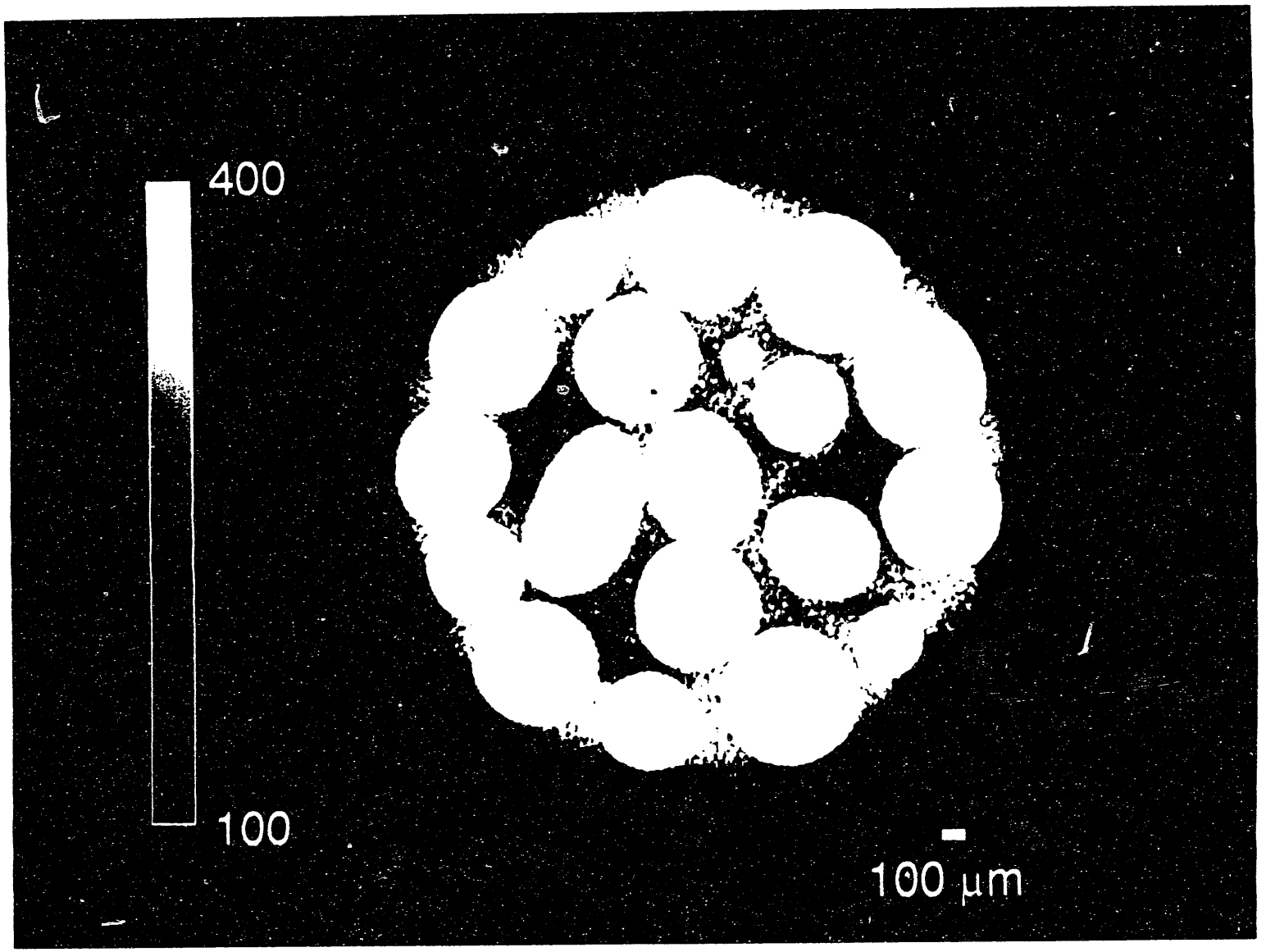

Figure 5

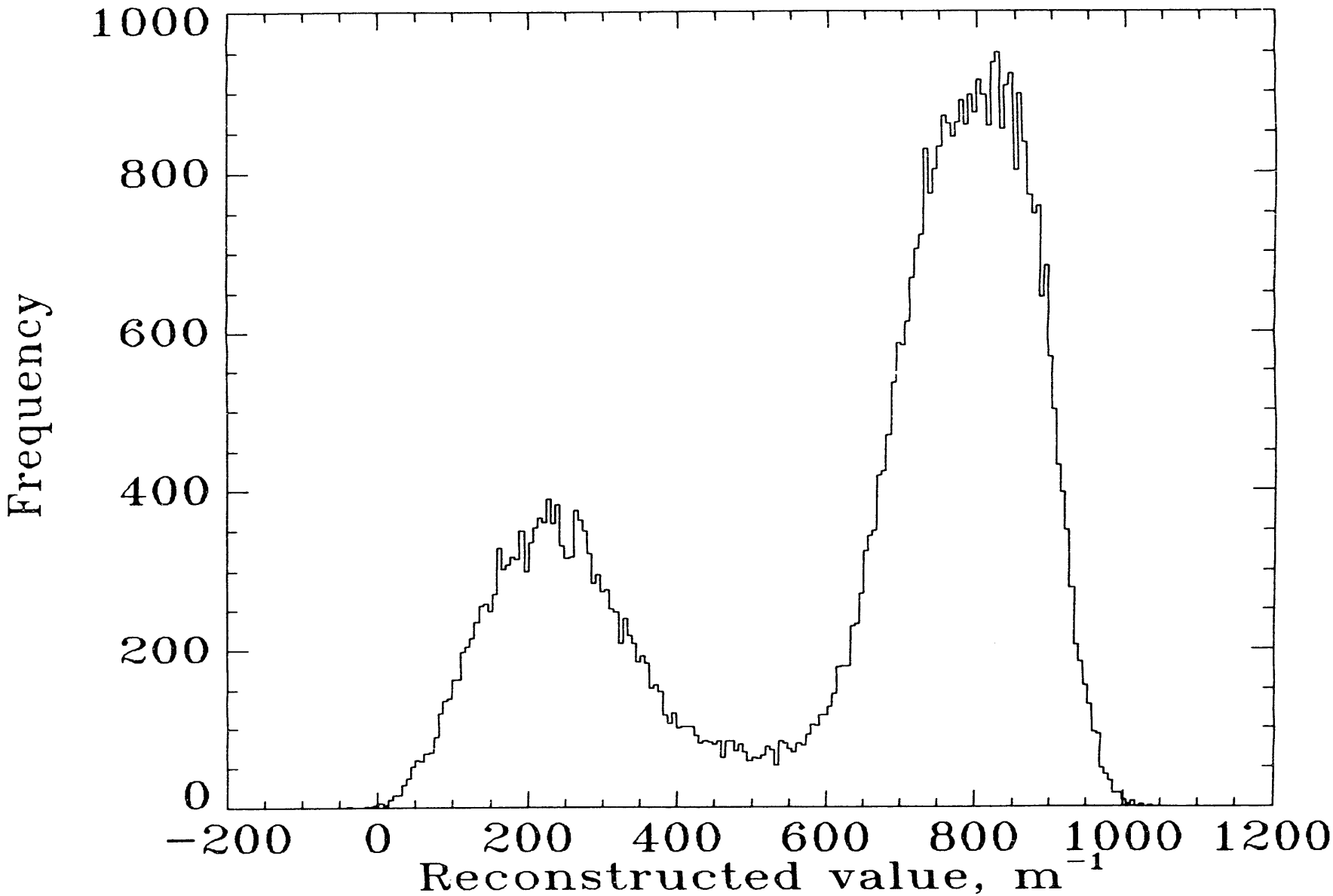
1000
800
600
400
200
0
Frequency
−200
0
200
400
600
800
1000
1200
Reconstructed value, m^{-1}

Figure 6

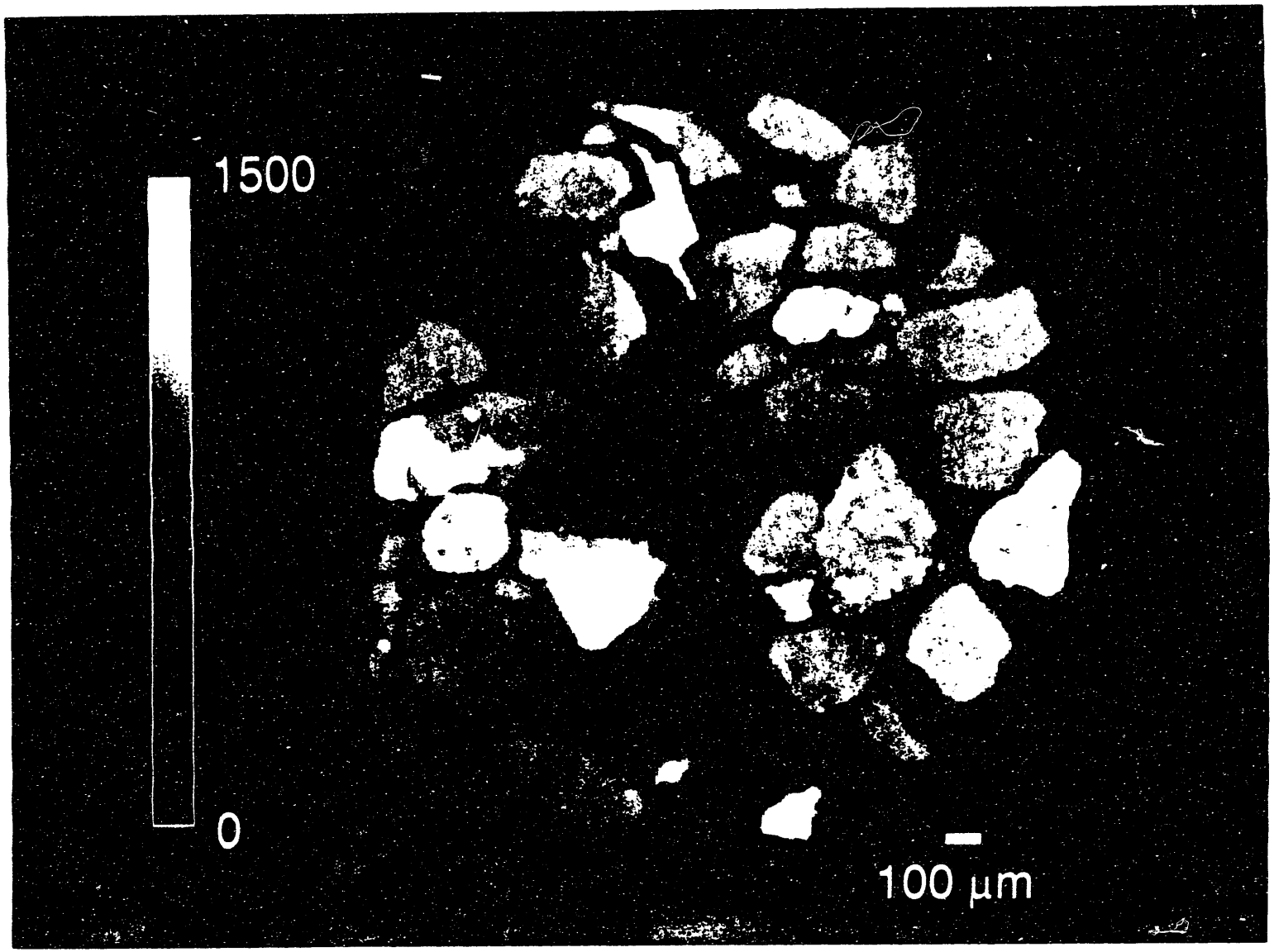

Figure 7

END

DATE FILMED

6/17/93